

1 Measurement of Muon neutrino Charged-Current 2 Neutral Pion Production at ICARUS

3 Lane Kashur

4 April 28, 2025

5 **Abstract**

6 Begin abstract

7
8 End abstract

9 **Contents**

10	1 Introduction	2
11	1.1 Measurement	2
12	1.2 Data and Monte Carlo Samples	3
13	1.2.1 Data Quality Cuts	3
14	1.2.2 Unblinding Strategy	4
15	2 ν_μ CC π^0 Selection	4
16	2.1 Signal Definition	4
17	2.2 Selection Cuts	4
18	2.3 Selection Performance	5
19	2.4 Reconstructed Observables	7
20	2.4.1 Muon Observables	7
21	2.4.2 Neutral Pion Observables	7
22	3 Systematic Uncertainties	8
23	3.1 Flux Uncertainties	10
24	3.2 Interaction Model Uncertainties	10
25	3.3 Detector Uncertainties	12
26	3.4 Reconstructed Observables with Systematic Uncertainties	12
27	4 Cross Section Measurement	12
28	4.1 Cross Section Extraction Procedure	12
29	4.2 Results	12

30	5 Conclusions	12
31	Appendices	12
32	A Data Quality Cuts	12
33	B Machine Learning Reconstruction	12
34	B.1 Point Classification	13
35	B.2 Formation of Particles and Interactions	13
36	B.3 Post-Processors	13
37	C Energy Reconstruction	13
38	C.1 Tracks	13
39	C.2 Showers	14

40 1 Introduction

41 Serving as the far detector for the Short-Baseline Neutrino (SBN) Program,
42 ICARUS is poised to address anomalous results from the LSND and MiniBooNE
43 experiments, where excesses of electron-like events could possibly be interpreted
44 as originating from light sterile neutrinos. One key to resolving these anomalies
45 is the search for electron neutrinos in a predominantly muon neutrino beam,
46 for which ICARUS and other detectors in the SBN suite rely on liquid-argon
47 time projection chamber (LArTPC) technology. With excellent calorimetry
48 and fine-grained spatial resolution, LArTPCs enable ICARUS to make precise
49 measurements of electron neutrino interactions as part of a robust neutrino
50 oscillation program.

51 Equally important to the success of ICARUS is characterization of back-
52 grounds that can mimic the electron neutrino appearance signal. Primary
53 among these backgrounds is the production of neutral pions, or π^0 s, which decay
54 electromagnetically to photons. π^0 production is mostly attributed to baryon
55 resonance (RES) in neutrino-nucleon interactions that occur at few-GeV scale,
56 which is also the energy at which the upcoming Deep Underground Neutrino
57 Experiment (DUNE) neutrino beam peaks at. An ICARUS analysis centered
58 around neutral pions therefore not only informs us about the SBN Program's
59 most significant background, but also provides a probe for the types of neutrino
60 interactions expected at next-generation oscillation experiments.

61 1.1 Measurement

62 In this document, we report the measurement of muon neutrino charged-current
63 interactions with a single π^0 in the final state on argon, hereafter referred to as
64 ν_μ CC π^0 interactions:

$$\nu_\mu + Ar \rightarrow \mu^- + \pi^0 + 0\pi^\pm + X. \quad (1)$$

Here, X represents any final state particles that are not muons or charged pions. The omission of charged pions in the final state aims to exclude charged-current coherent pion production from the analysis, therefore allowing the cross section measurement to probe the resonant production mode that is more relevant to the SBN Program.

Few charged-current π^0 measurements exist on liquid argon, and a high statistics cross section measurement of this channel at ICARUS will help constrain uncertainties in modeling resonant neutrino-nucleon interactions. We present single differential cross section measurements of ν_μ CC π^0 interactions as a function of muon and neutral pion kinematic variables, namely the momentum and angle with respect to the neutrino beam for each particle. Event selection is carried out with a novel machine-learning reconstruction pipeline, where high purity and excellent resolution in reconstructed variables enable the extraction of a precise, finely-binned cross section.

1.2 Data and Monte Carlo Samples

This analysis utilizes ICARUS data collected from the Booster Neutrino Beam (BNB) between winter 2022 and spring 2023 (ICARUS Run 2). This collection period corresponds to approximately 2.05×10^{20} protons on target (POT). The analysis can be easily extended to the Neutrinos at the Main Injector (NuMI) beam, and will be in the future as data processing and treatment of systematic uncertainties allows. Data is processed through the ICARUS reconstruction chain (see Appendices A & B) with *icaruscode* software version v09.89.01.01.

Monte Carlo simulation consisting of BNB neutrinos (produced with GENIE) and cosmics (produced with CORSIKA) is used to assess selection performance. This Monte Carlo sample corresponds to 1.74×10^{10} POT. To evaluate the impact from cosmic activity that occurs within the $1.6 \mu s$ BNB beam gate, off-beam data is used. A summary of production streams used in this analysis is shown in Table 1.

Table 1: Data/Simulation Productions used for ν_μ CC π^0 analysis.

	Production	POT
Data (on-beam)	BNB Run 2 On-Beam Majority Trigger	2.05×10^{20}
Data (off-beam)	BNB Run 2 Off-Beam Majority Trigger	N/A
Simulation	BNB ν + Cosmics	1.74×10^{20}

1.2.1 Data Quality Cuts

Not yet implemented

To ensure the data used in this analysis is of physics quality, a number of data quality cuts are enforced. Namely, any data collection runs that were subject to DAQ issues or happened during detector hardware updates are removed from consideration. Additionally, cuts are made to avoid detector features that are

yet to be modeled in simulation, including a field cage short in the EE TPC and a cable hanging in the active volume of the WW TPC. A full description of all data quality cuts used in this analysis can be found in Appendix A.

1.2.2 Unblinding Strategy

The official blinding policy of the ICARUS collaboration (doc-db 34523) states that 90 percent of data is to remain blinded until any analysis is finalized. To comply with this policy, all analysis toward the ν_μ CC π^0 cross section measurement shown in this document only uses the 10 percent of Run 2 data that has been unblinded. An exception has been made for data collection run 9435, which has been completely unblinded for the purpose of visual scanning.

Pending approval from the physics coordinators and event selection working group, we request access to...(To-do)

2 ν_μ CC π^0 Selection

2.1 Signal Definition

The ν_μ CC π^0 signal definition encompasses charged-current neutrino interactions occurring within the fiducial volume of the detector and containing

- exactly one primary muon ($p_\mu \geq 226$ MeV/c)
- exactly zero primary charged pions ($E_{\pi^\pm} \geq 25$ MeV)
- exactly one primary neutral pion
- any number of particles that are not muons or pions.

The momentum/energy requirements for muons and charged pions are phase space constraints to ensure tracking thresholds are met and purity is optimized. This signal definition applies to final state particles, or particles exiting the target nucleus post-final state interactions (FSI). The fiducial volume requirement applies to the neutrino interaction vertex, which must be 25 cm from detector boundaries in the drift and vertical directions, 30 cm from the upstream detector face, and 50 cm from the downstream face.

2.2 Selection Cuts

When selecting ν_μ CC π^0 interactions, cuts are made on various reconstructed outputs to narrow the list of candidate interactions. Included are cuts on:

- Fiducial volume: Reconstructed vertex is required to be inside fiducial volume (defined in signal definition).
- Flash time: Interaction is associated with an optical flash that is in-time with BNB beam gate, as determined by the OpT0Finder algorithm.

- 133 • Base Topology: Interaction contains
 - 134 – Exactly one primary muon ($p_\mu \geq 226$ MeV/c)
 - 135 – Exactly zero primary charged pions ($E_{\pi^\pm} \geq 25$ MeV)
 - 136 – Two or three primary photons ($E_\gamma \geq 20$ MeV)
- 137 • Leading Photon: Highest energy photon has $E_\gamma \geq 40$ MeV
- 138 • Neutral pion mass: Invariant diphoton mass < 400 MeV in order to reject
 - 139 η mesons.

140 Note that in the case of three primary photons meeting the above selection
 141 criteria, the photon pair with diphoton invariant mass closest to that of the
 142 true π^0 mass is chosen to belong to the candidate π^0 .

143 2.3 Selection Performance

144 Selection performance is assessed using the BNB ν + Cosmic MC sample and
 145 off-beam BNB Run 2 data. The metrics that have been evaluated are efficiency -
 146 the fraction of true signal interactions that are matched to selected interactions,
 147 and purity - the fraction of selected interactions that are matched to true signal
 148 interactions. Efficiency and purity for each selection cut are shown in Table 2.

Table 2: Purity and efficiency for ν_μ CC π^0 Selection Cuts

Selection Cut	Efficiency [%]	Purity [%]
No Cut	xx	xx
In-Time Flash	xx	xx
Fiducial Volume	xx	xx
Base Topology	xx	xx
Leading Shower	xx	xx
$m_{\gamma\gamma} < 400$ MeV/c ²	72	83

149 Selection efficiency as a function of the cross section variables introduced in
 150 Section 1 are shown in Figure 1, showing that efficiency is largely flat across
 151 the signal phase space. Both inefficiencies and impurities in the selection are
 152 driven by particle identification (PID) failures, as shown in confusion matrices
 153 for true signal particles (Figure 2a) and reconstructed selected particles (Figure
 154 2b). Additionally, background topologies can be seen in Section 2.4.

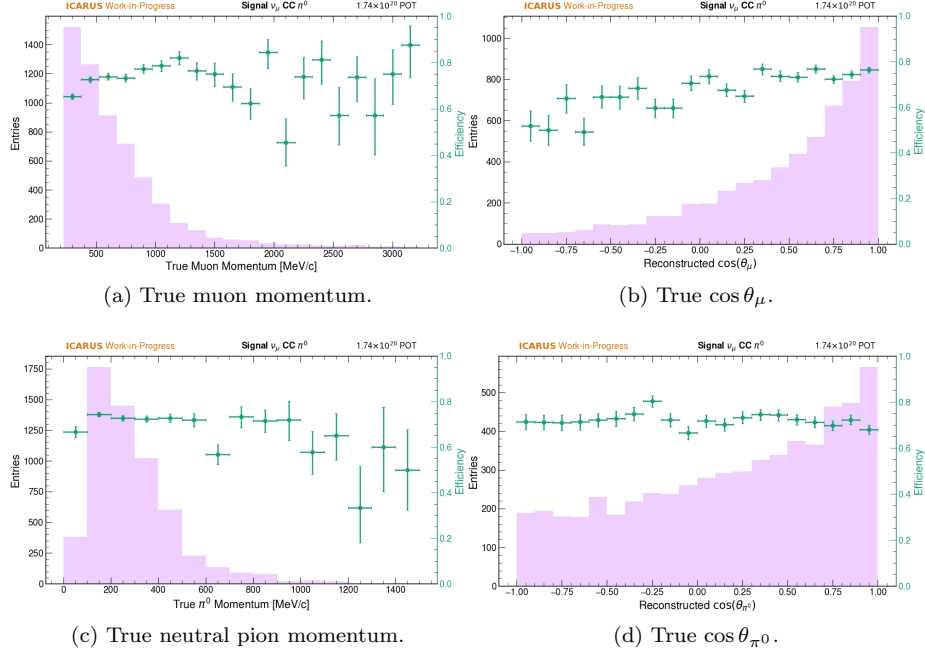


Figure 1: Confusion matrices for particle identification, as determined by the SPINE machine-learning chain.

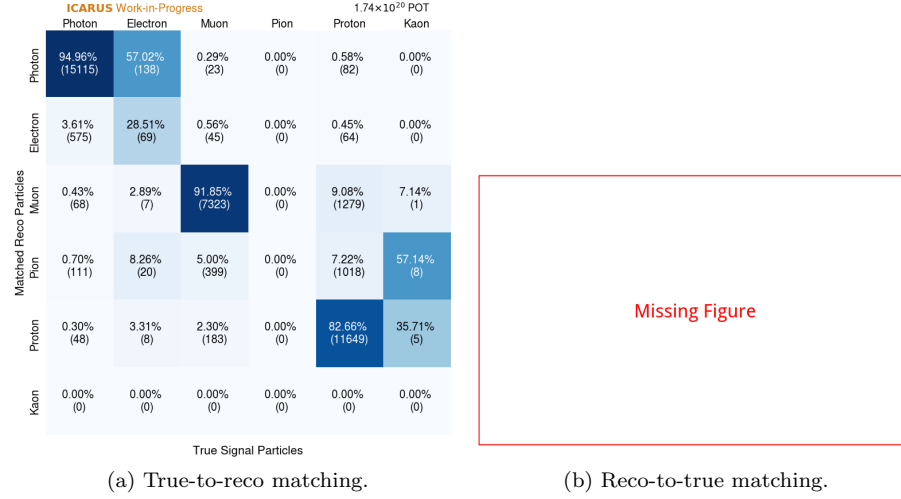


Figure 2: Confusion matrices for particle identification, as determined by the SPINE machine-learning chain.

2.4 Reconstructed Observables

In this section, the kinematic observables used in the single differential cross section measurement are highlighted. Included are the momenta of the final state muon and neutral pion, as well as the angles these particles make with the BNB. An additional variable, the invariant diphoton mass, is examined as it serves as a useful standard candle in the calibration of the electromagnetic shower energy scale.

2.4.1 Muon Observables

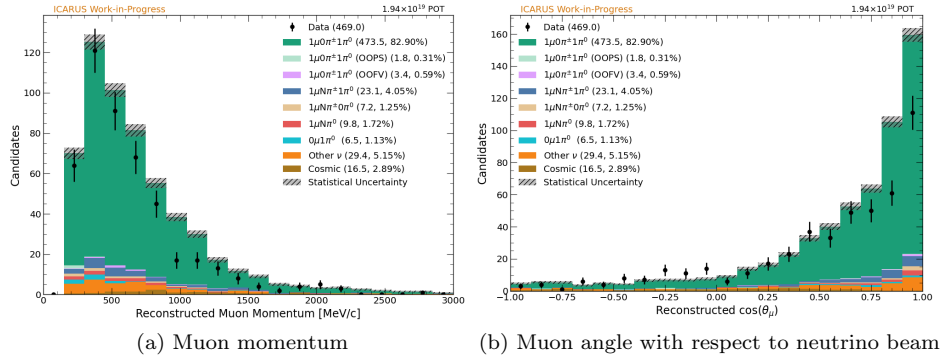


Figure 3: Muon observables chosen for analysis

2.4.2 Neutral Pion Observables

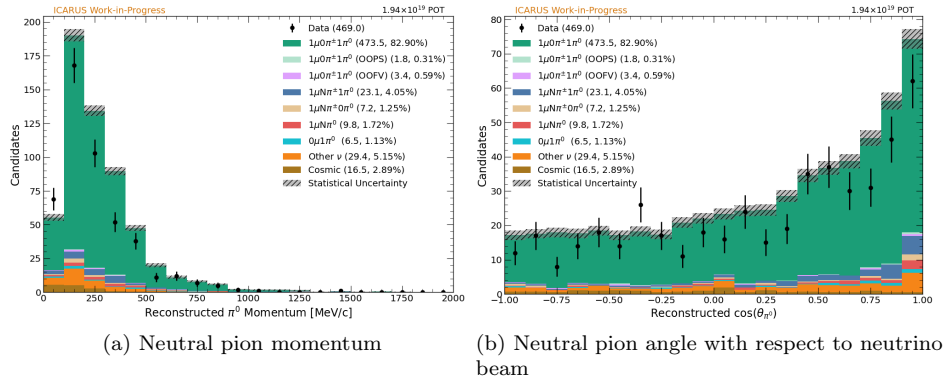


Figure 4: Neutral pion observables chosen for analysis

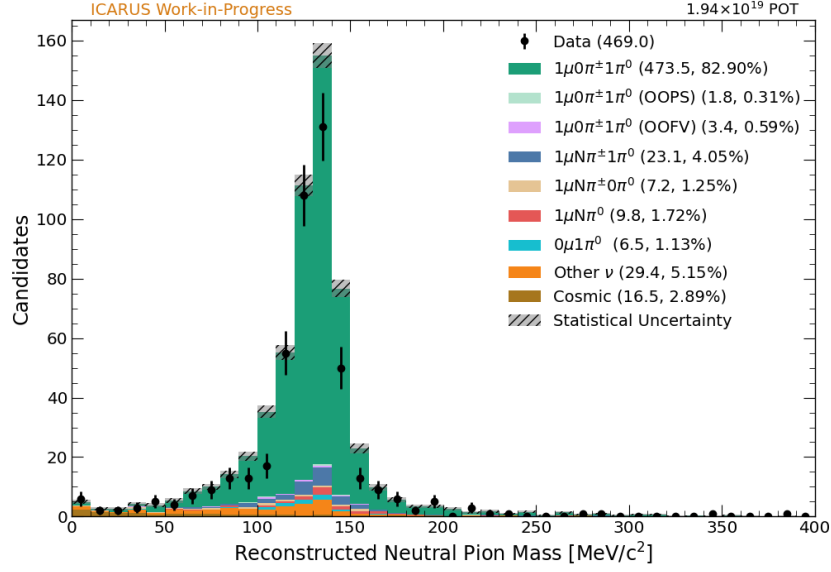


Figure 5: Neutral pion invariant mass

3 Systematic Uncertainties

The systematic uncertainties relevant to this analysis are divided into three categories: (1) beam flux, (2) interaction modeling, and (3) detector response modeling. Error bands on reconstructed observables for these systematic uncertainties are shown in Figure xx, and each source of uncertainty is discussed in further detail below.

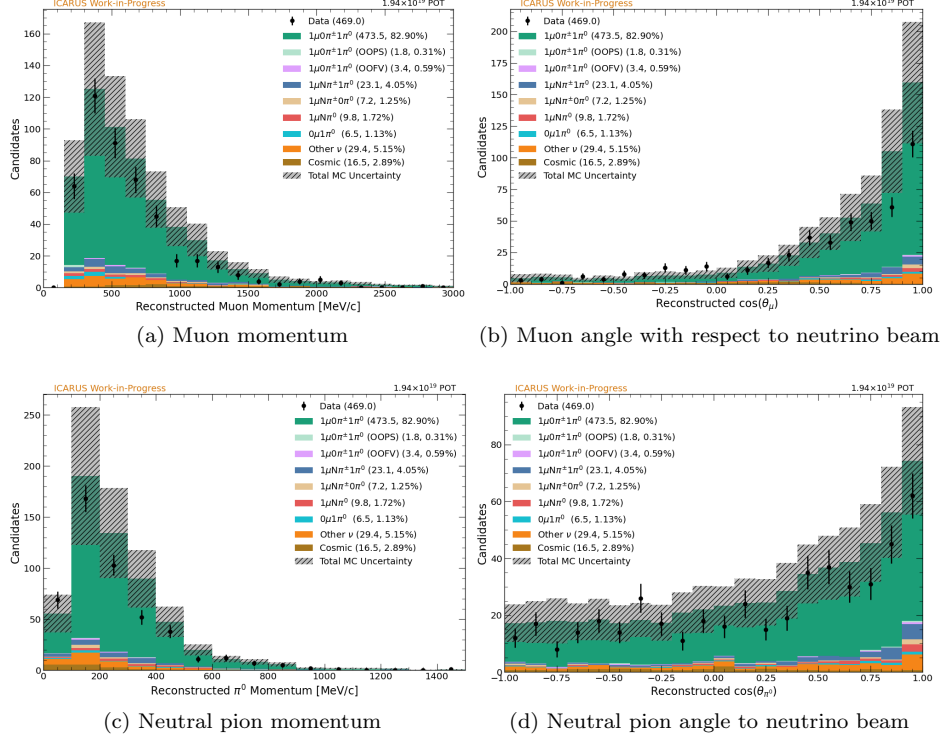


Figure 6: Observables chosen for analysis

Beam flux and interaction modeling uncertainties are evaluated with a many-universes technique, where parameters affecting the probability of an interaction occurring are varied within their uncertainties in a number of “universes”. One thousand universes are employed in this analysis, each of which is used to assign weights to neutrino interactions in order to assess the impact of the parameter variations. A covariance matrix then captures the uncertainty on binned reconstructed observables by comparing event counts across different universes and the central value sample:

$$V_{ij} = \frac{1}{N} \sum_k^N (M_i^k - M_i^{CV})(M_j^k - M_j^{CV}) \quad (2)$$

where N is the number of universes, M_i^k (M_j^k) is the measured event count for bin i (j) in the k th universe, and M_i^{CV} (M_j^{CV}) is the measured event count for bin i (j) in the central value universe.

Detector response modeling uncertainties are evaluated with a “uni-sim” technique, where elements of the detector response model are modified in dedicated variation samples.

3.1 Flux Uncertainties

The BNB flux at ICARUS is based on predictions from the MiniBooNE collaboration, which used the Geant4 simulation tool kit to model the propagation of particles produced in proton beam-target interactions [1]. Treatment of flux uncertainties, which arise from sources like hadron production, hadronic secondary interactions within the beam target, and beam focusing, are handled with a many-universes technique. The full set of beam flux uncertainties studied in this analysis are shown in Table 3.

Table 3: Flux uncertainties for ν_μ CC π^0 selection

Uncertainty	Description	Scale [%]
kminus	K^- production in beam target	0
kplus	K^+ production in beam target	0
kzero	K^0 production in beam target	0
pminus	π^- production in beam target	0
piplus	π^+ production in beam target	0
expskin	Skin Depth	0
horncurrent	Horn Current	0
nucleoninexsec	Nucleon inelastic re-scattering in beam target	0
nucleonqexsec	Nucleon QE re-scattering in beam target	0
nucleontotxsec	Nucleon total re-scattering in beam target	0
pioninexsec	π inelastic re-scattering in beam target	0
pionqexsec	π QE re-scattering in beam target	0
piontotxsec	π total re-scattering in beam target	0

3.2 Interaction Model Uncertainties

Neutrino-argon interactions are simulated with the GENIE neutrino event generator, specifically version 3.4 with model configuration AR23_20i_00_00 - known colloquially as the “DUNE tune”. GENIE provides reweightable parameters that can be used to assess interaction model uncertainties via the many-universes approach, similar to the handling of flux uncertainties discussed previously. The full set of interaction model uncertainties studied in this analysis are shown in Table 4

Table 4: Interaction model uncertainties for ν_μ CC π^0 selection

Uncertainty	Description	Scale [%]
ZExpAVariationResponse	Z-expansion of axial form factor for CCQE interactions	0
RPA_CCQE	RPA suppression for CCQE interactions	0
CoulombCCQE	Value of Coulomb potential in corrections for CCQE interactions	0
NormCCMEC	Normalization for CCMEC interactions	0
NormNCMEC	Normalization for NCMEC interactions	0
NCELVariationResponse	Variation of the dipole form factor for NCEL interactions	0
CCRESVariationResponse	Variation of the dipole form factor for CCRES interactions	0
NCRESVariationResponse	Variation of the dipole form factor for NCRES interactions	0
NonRESBGvpCC1pi	Scale factor for non-resonant ν - p CC 1π background	0
NonRESBGvpCC2pi	Scale factor for non-resonant ν - p CC 2π background	0
NonRESBGvpNC1pi	Scale factor for non-resonant ν - p NC 1π background	0
NonRESBGvpNC2pi	Scale factor for non-resonant ν - p NC 2π background	0
NonRESBGvnCC1pi	Scale factor for non-resonant ν - n CC 1π background	0
NonRESBGvnCC2pi	Scale factor for non-resonant ν - n CC 2π background	0
NonRESBGvnNC1pi	Scale factor for non-resonant ν - n NC 1π background	0
NonRESBGvnNC2pi	Scale factor for non-resonant ν - n NC 2π background	0
NonRESBGvbarpCC1pi	Scale factor for non-resonant $\bar{\nu}$ - p CC 1π background	0
NonRESBGvbarpCC2pi	Scale factor for non-resonant $\bar{\nu}$ - p CC 2π background	0
NonRESBGvbarpNC1pi	Scale factor for non-resonant $\bar{\nu}$ - p NC 1π background	0
NonRESBGvbarpNC2pi	Scale factor for non-resonant $\bar{\nu}$ - p NC 2π background	0
NonRESBGvbarnCC1pi	Scale factor for non-resonant $\bar{\nu}$ - n CC 1π background	0
NonRESBGvbarnCC2pi	Scale factor for non-resonant $\bar{\nu}$ - n CC 2π background	0
NonRESBGvbarnNC1pi	Scale factor for non-resonant $\bar{\nu}$ - n NC 1π background	0
NonRESBGvbarnNC2pi	Scale factor for non-resonant $\bar{\nu}$ - n NC 2π background	0
RDecBR1gamma	Scale factor for $X + 1\gamma$ branching fraction	0
RDecBR1eta	Scale factor for $X + 1\eta$ branching fraction	0
COHVariationResponse	Normalization for coherent interactions	0
DISBYVariationResponse	Variation of parameters in Bodek-Yang DIS model	0
FSI_pi_VariationResponse	Variation of FSI parameters involving pions	0
FSI_N_VariationResponse	Variation of FSI parameters involving nucleons	0

200 **3.3 Detector Uncertainties**

201 **3.4 Reconstructed Observables with Systematic Uncer-** 202 **tainties**

203 **4 Cross Section Measurement**

204 **4.1 Cross Section Extraction Procedure**

205 **4.2 Results**

206 **5 Conclusions**

207 **References**

- 208 [1] A. A. A.-A. et al. (MiniBooNE Collaboration), “Neutrino flux prediction
209 at miniboone”, Phys. Rev. D 79, 072002 (2009).
- 210 [2] F. Drielsma, K. Terao, and L. D. and Dae Heun Koh, “Scalable, end-to-end,
211 deep-learning-based data reconstruction chain for particle imaging detec-
212 tors”, (2021).

213 **Appendices**

214 **A Data Quality Cuts**

215 **B Machine Learning Reconstruction**

216 Reconstruction of neutrino events is handled by the end-to-end, machine-learning
217 based reconstruction chain known as SPINE (Scalable Particle Imaging with
218 Neural Embeddings) [2]. As input, SPINE takes an image of 3D charge de-
219 positions within the detector, which is then operated on by a series of neural
220 networks to carry out point classification and formation of particle and interac-
221 tion objects.

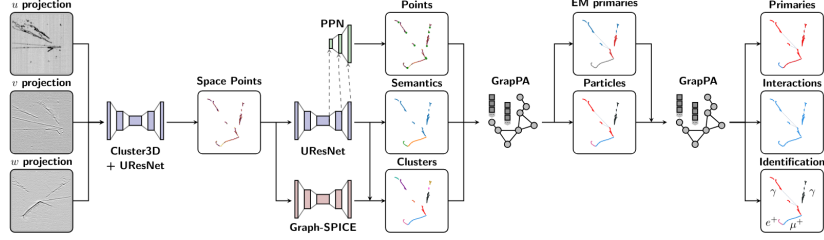


Figure 7: The SPINE reconstruction chain.

B.1 Point Classification

Point classification refers to the classification of 3D space points into abstract particle classes and the identification of points of interest. Convolution neural networks (CNNs) are used for these tasks, beginning with the removal of tomographic reconstruction artifacts by the

B.2 Formation of Particles and Interactions

B.3 Post-Processors

C Energy Reconstruction

Energy reconstruction refers to the estimation of initial kinetic energy of particles in the ν_μ CC π^0 selection. From this, reconstructed observables like momentum can then be calculated.

C.1 Tracks

To estimate the energy of tracks made by charged particles (e.g. muons and charged pions), a “best estimate” approach is taken. For tracks contained within the active detector volume, energy is calculated using the Continuous Slowing Down Approximation (CSDA) that relates a particle’s kinetic energy to its range in a material. For energy estimation of exiting tracks, the degree of multiple coulomb scattering (MCS) along the track is instead used. Figure XX shows how each energy estimate compares with true kinetic energy for simulated BNB muons from neutrino interactions.

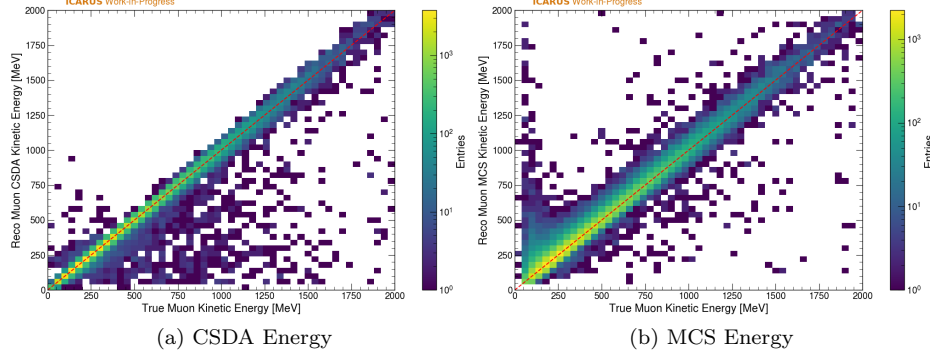


Figure 8: Track energy reconstruction for muons from BNB simulation

C.2 Showers

Unlike charged particles, neutral pions do not directly ionize the detector medium. The neutral pion energy must therefore be inferred from the electromagnetic showers instigated by the photons it decays to. Shower energy is estimated calorimetrically by summing charge depositions belonging to the shower and accounting for various detector effects:

$$E_{shower} = W_i \left[\frac{MeV}{e^-} \right] \cdot C_{cal} \left[\frac{e^-}{ADC} \right] \cdot C_{adj} \cdot \frac{1}{R} \cdot \sum_{dep} e^{\frac{t_{drift}}{\tau}} \cdot dep[ADC], \quad (3)$$

where

W_i is the work function for argon

C_{cal} converts charge units from ADC to electrons

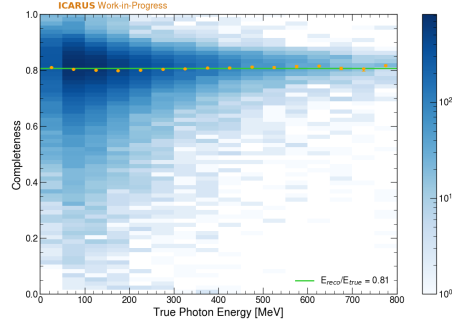
C_{adj} accounts for missing energy due to subthreshold charge and clustering effects in reconstruction

R is the recombination factor

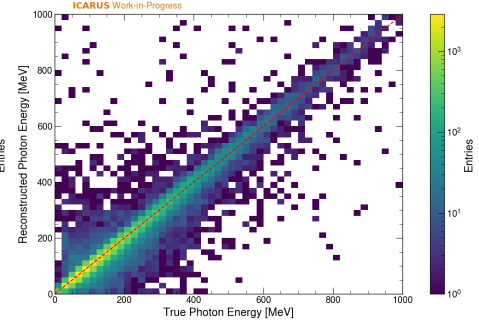
τ is the electron lifetime

dep is charge in units of ADC.

The shower correction factor, C_{adj} , is derived from a study of contained photons in simulation. Figure 9a shows the ratio of reconstructed photon energy (from Equation 3) to true photon energy. As this ratio is mostly flat across different energies, a constant correction factor is chosen. Reconstructed photon energy is again compared to true photon energy in Figure 9b, showing agreement after the correction factor is applied. It is also worth noting that since the signal definition for this analysis does not require showers to be contained, an additional correction factor is needed to correct for missing energy in exiting showers. A study for deriving this factor is ongoing with results expected soon.



(a) Shower Energy Adjustment Factor



(b) Post-Shower Energy Adjustment

Figure 9: Track energy reconstruction for muons from BNB simulation